

## **Performance Assessment of Solar based Air Conditioning System**

**S. Mishra, S. Singh\***

Department of Electrical Engineering, Shri Ramswaroop Memorial University, Lucknow 226005, Uttar Pradesh, India

Received 30 June 2021, accepted in final revised form 27 September 2021

### **Abstract**

The conventional air-conditioning system suffers from (i) harmonic distortion at the input ac side due to extensive use of nonlinear loads and (ii) not being friendly with the environment and climate. In this paper, a conventional air conditioning system (ACS), which uses a single-phase ac supply, is replaced by a solar-powered ACS to mitigate mentioned shortcomings. Due to the non-availability of solar energy during night/low-intensity levels, a battery and a dc-dc converter are used to maintain constant voltage, a prime requirement for ACS. Further, if an ac supply is used during the daytime, the battery is not required. Thus, a self-sustained solar-powered air conditioner of a capacity of 1.5 tons is designed here. The solar system is designed using Simulink, and various parameters such as torque and speed are being measured to study & analyze the solar-based ACS. The designed air conditioner gives an acceptable performance despite the variation of solar irradiations.

*Keywords:* Solar energy; ACS; Performance; Photovoltaic (PV).

© 2022 JSR Publications. ISSN: 2070-0237 (Print); 2070-0245 (Online). All rights reserved.  
doi: <http://dx.doi.org/10.3329/jsr.v14i1.54429> J. Sci. Res. **14** (1), 167-177 (2022)

## **1. Introduction**

Electricity is the prime requirement for a human being in the current era. As the conventional sources of energy are limited, alternate energy sources are now in demand. These energy sources are self-sustainable & environment safe [1]. Using these renewable sources, conversion of electrical energy reduces pollution caused by fossil fuels and improves the total generation [2-6].

The generation of electricity through solar energy is widely used in India due to climatic conditions. Various photovoltaic panels are connected in series and/or parallel to generate energy through solar to achieve high voltage/current [7]. As the intensity of the Sun varies, the generated power is varied; therefore, the power of the system is optimized when the load characteristic changes to keep the power transfer at high efficiency.

This load characteristic is called maximum power point (MPP). A standalone solar PV array-fed water pumping system has been described in which solar PV array alters solar energy into electrical energy [8]. A dc converter is required to transfer maximum power from the solar PV module to the load by changing the duty cycle. For this purpose,

---

\* Corresponding author: [shikha.ec@srmu.ac.in](mailto:shikha.ec@srmu.ac.in)

various isolated/non-isolated converter configurations may be used. Generally, non-isolated boost and buck-boost converter configurations have been used. However, the boost converter is mainly used to boost output voltage regulation to the desired level [9]. A battery is used along with a charge controller to provide energy in the absence of solar sunshine. It is connected in parallel to the boost converter through a bidirectional converter [10,11]. The bidirectional converter is used for interfacing between the battery bank and solar PV system for continuous flow of power [12-14]. The inverter is used to drive the motor of ACS [15,16]. A novel PV inverter scheme based on single input and multiple outputs with multilevel inverter is used for harmonic distortion reduction as presented by Bhukya *et al.* [17]. To track power from the solar PV module, an adapted Aalborg inverter is used and is presented by Wang *et al.* [18]. A separate solar air-cooling system with DC motors to drive the pump and air blower fan load attached to their particular shafts is implemented [19]. A new crowded plant height optimization algorithm is introduced for solar PV maximum power point tracking [20]. The design, modeling, and performance analysis of bidirectional solar inverter linked to the grid are presented using the maximum power extraction technique [21].

Power quality is one of the major issues which adversely affect the system. An adaptively switched filter compensator using a PID controller has been described to enhance the powerful qualities of the Microgrid [22]. The latest PWM technique has been introduced to lower the line frequency harmonics in single-phase loads incorporating a PV-micro inverter system [23]. It mitigates double line frequency harmonics by using only a small dc-link capacitor. The conventional ACS can be built using different converters using DBR in the front end [24-26]. Various without bridge converters for ACS have been discussed [27,28]. Utilizing solar energy to operate an ACS has been presented by Das *et al.* [29].

In this paper, conventional AC supply is replaced by solar radiation, and battery and controller are incorporated to maintain constant voltage in ACS. This arrangement reduces the harmonic emission at the front end due to conventional supply, reduces environmental pollution, and is self-sustainable.

## **2. Schematic Diagram of Solar-Based ACS**

The schematic diagram of solar-based ACS is shown in Fig. 1. The solar PV system energizes the boost converter to attain MPP by controlling the duty cycle. The voltage and current of the PV array are given to the MPP controller, and error is compared to the sawtooth generator to generate PWM pulses for the boost converter. In addition, a battery is used along with a controller to provide energy during the absence of solar radiation and maintain a constant voltage. To maintain battery charging, the output voltage of the boost converter is compared with constant, which is given to the PI controller, and generated pulses are given to the bidirectional converter. A VSI is controlled by electronic switching, and its function is to invert the voltage obtained from solar PV modules. The output of the inverter is given to the BLDC motor to drive an ACS.

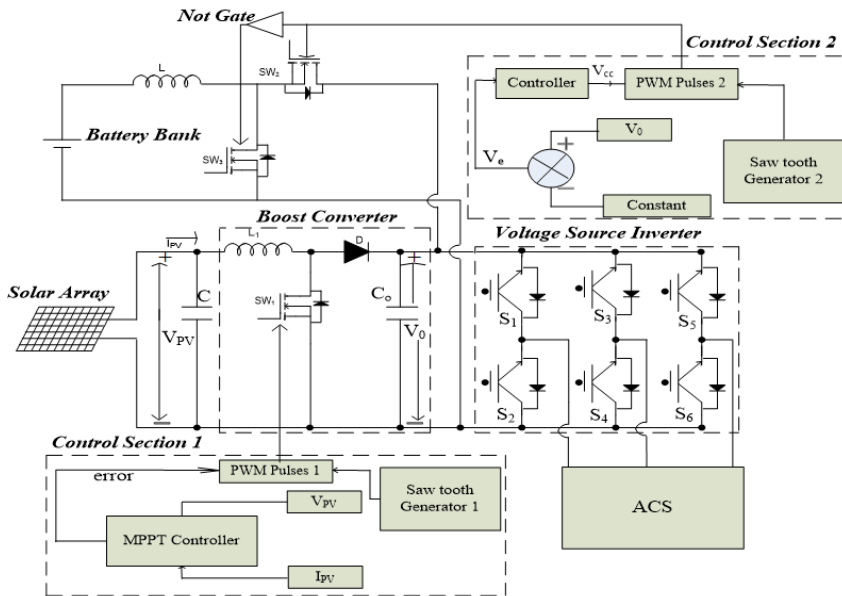


Fig. 1. Schematic of solar-based ACS.

### 3. Design of Solar-Based ACS

The solar-based ACS consists of the solar PV system, boost converter, battery, charge controller, and inverter followed by a motor to drive the AC. The components' designs of each system are carried out to model the solar-based ACS and are given in the following subsections.

#### 3.1. Design of solar array

The solar panel is designed by using solar cell equations [3]. The base equation between the current and voltage is given as

$$I = I_{ph} - I_0(e^{qV/kT} - 1) = I_{ph} - I_d \tag{1}$$

$$V_{OC} = \left(\frac{nkT}{q}\right) \ln\left(\frac{I}{I_0}\right) \tag{2}$$

The PV array is designed for 3 kW power. The specifications have been tabulated in Table 1.

Table 1. PV characteristics of designed solar-based ACS.

Parameter	Value
Short-circuit current [A]	$I_{SC}= 8.21$
Open-circuit voltage [V]	$V_{OC}= 32.9$
MPP voltage [V]	$V_{mp}= 26.3$
MPP current [A]	$I_{mp}= 7.61$
Series resistance ( $\Omega$ )	$R_s= 0.2218$
Parallel resistance ( $\Omega$ )	$R_p= 15.405$
Photo voltaic current [A]	$I_{PV}= 8.214$
Sample time (sec)	$t= 10e^{-6}$
Number of cells per module	$N=54$
Number of series-connected modules	$N_{ser}=8$
Number of parallel modules	$N_{par}=2$

### 3.2. Design of boost converter

The input voltage of the boost converter is the output voltage of the PV array and is given by

$$V_{PV} = (V_{mp} * 8) = (26.3 * 8) = 210V \quad (3)$$

In steady-state, the value of input inductor at 20 kHz switching frequency is given as

$$L_1 = \frac{nV_{in}T_s}{4\Delta I_{L2}} = \frac{0.42 * 210V * 0.00005}{4 * 0.837} = 1.3mH \quad (4)$$

The output capacitor value is calculated considering 2% of allowable output voltage ripple is given as

$$C_d = \frac{I_o}{2\omega\Delta V_o} = \frac{8.37A}{2 * 314Hz * 7.2V} = 1.85mF \quad (5)$$

### 3.3. Design of battery

The battery acts as a source to run the ACS when the supply is not present. The battery bank is designed at a nominal voltage of 320 V at a rated capacity of 8 Ah. The specification of the battery bank is given in Table 2. To control the battery charging, the bidirectional converter is used to maintain power flows in both ways, i.e., from PV array to battery bank and vice-versa. A bidirectional converter has two switches acting one at a time. The switching frequency of the bidirectional converter is maintained at 20 kHz. The internal resistance and snubber resistance of the switches are 0.001 and 100 k $\Omega$ , respectively.

### 3.4. Design of VSI

The three-phase voltage source inverter is designed to invert the voltage obtained by PV modules to act as an input to the motor. The internal and snubber resistance of VSI is

0.001  $\Omega$  and 5 k $\Omega$ , respectively, and IGBT/diodes are used as power electronic devices for constructing the VSI.

Table 2. Characteristics of designed battery.

Parameter	Value
Nominal voltage [V]	320
Rated capacity [Ah]	8
Initial state of charge [%]	80
Maximum capacity [Ah]	8.33
Fully charged voltage [V]	348.42
Nominal discharge current [A]	1.6

### 3.5. Design of BLDC motor

The ac voltage of VSI is given to the BLDC, which is designed for ACS. The simulation parameters of the BLDC motor are given in Table 3.

Table 3. Designed parameters of BLDC for ACS.

Parameters of BLDC	Value
Number of Phases	3
Stator Phase resistance $R_s$	18 $\Omega$
Stator phase inductance $L_s$	0.01 H
Back EMF flat area	120°
Viscous damping	0.4e-03 N.m.s

## 4. Performance of Solar Based ACS

The solar-based ACS is designed and modeled for the performance assessment under various solar irradiations to test the reliability and ruggedness. An ode45 solver is used to model the system in discrete time. PV voltage ( $V_{PV}$ ), current ( $I_{PV}$ ), and power ( $P_{PV}$ ) along with dc output voltage ( $V_{dc}$ ) of the boost converter are shown in Fig. 2. The panel's power is maintained constant around 2950 W (voltage of 217 V and current of 13.58 A). The output voltage of the boost converter is 360 V which also constantly verifies the design of the PV array and boost converter. DC output current of boost converter ( $I_{dc}$ ) and three-phase output voltage ( $V_{inv}$ ) of the inverter is shown in Fig. 3. The boost converter's dc output current varies from 0 to 9.6 A, while the three-phase inverter voltage varies from -360 to 360 V. The battery, along with the charge controller, is connected in parallel with the boost converter. The  $V_b$  and  $I_b$  are the voltage and current of the battery charge controller, respectively, while  $V_{bc}$  and  $I_{bc}$  are the voltage and current of the bidirectional converter, respectively. As shown in Fig. 4, the  $V_b$  and  $I_b$  are obtained as 329 V and 6.2 A, respectively. The voltage across bidirectional converter  $V_{bc}$  is 360 V, while the current of bidirectional converter  $I_{bc}$  varies from 0 to 6.6 A, respectively.

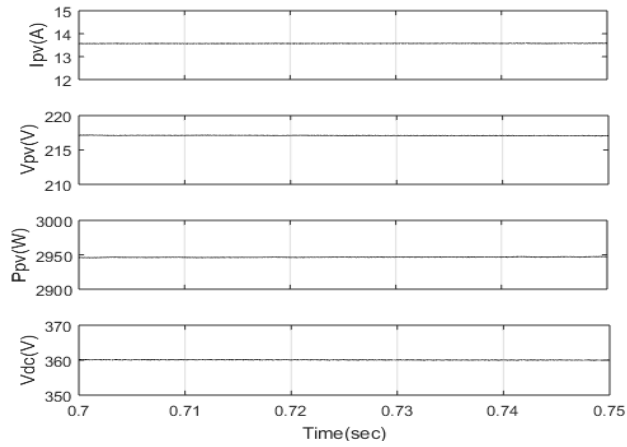


Fig. 2. PV current, PV voltage, PV power, and dc output voltage of solar-based ACS.

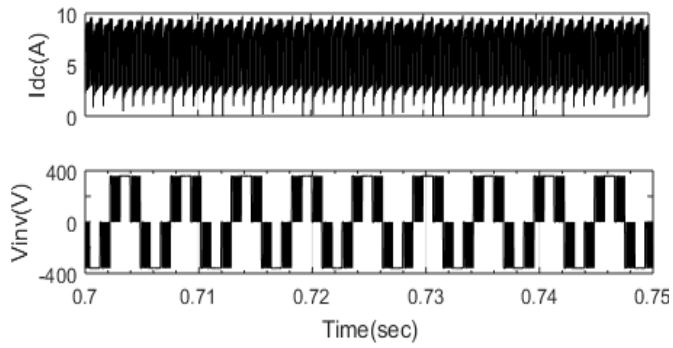


Fig. 3. DC output current and three-phase output voltage of inverter for solar-based ACS.

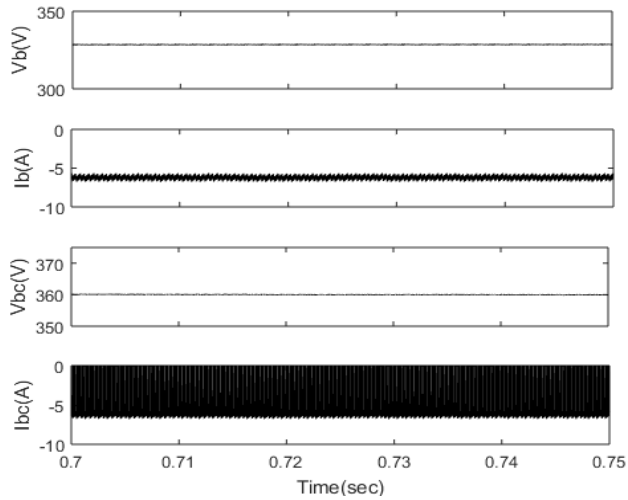


Fig. 4. Battery charge controller voltage, current, and bidirectional converter voltage and current.

The  $i_m$  and  $e_m$  are the stator current and electromotive force, respectively, while  $\omega$  and  $\tau$  are rotor speed and electromagnetic torque. As from Fig. 5, the stator current and emf of the motor are obtained as 3 A and 118 V, respectively. The rotor speed is 1874 rpm, constant, and torque varies from 2.4 to 3.6 Nm.

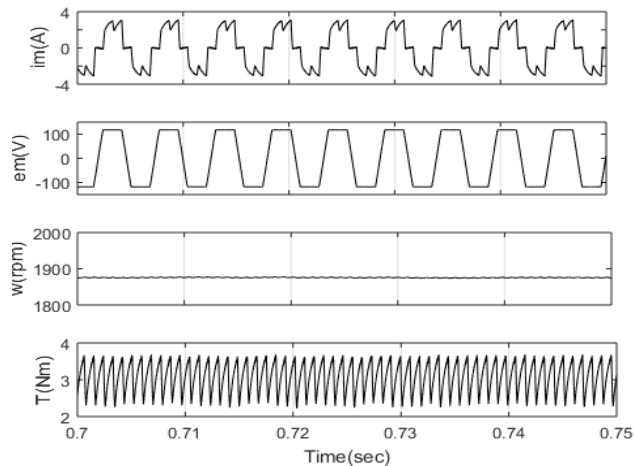


Fig. 5. Stator current, electromotive force, rotor speed, and electromagnetic torque.

The solar radiation is varied, and the performance of the ACS has been studied in Figs. 6-8 for solar irradiance of 800, 400 and 0  $\text{w/m}^2$  respectively. As from Fig. 6, for the solar irradiance of 800  $\text{w/m}^2$  the PV voltage and dc output voltage are 217 and 360 V, respectively, while the current falls to 10.64 A, the power of PV decreases. The battery's voltage observes at 327 V while the current reduces to 4.3 A, and the bidirectional converter current varies from 0 to 4.8 A. The rotor speed comes out to be 1874 rpm.

Fig. 7 shows the performance of ACS when the solar irradiance reduces to 400  $\text{w/m}^2$ . The PV and dc output voltage are observed at 216.7 and 360 V, respectively, while the current falls to 4.65A, reducing PV power. The battery's voltage observes at 325 V while its current reduces to 0.5 A. Bidirectional converter's current varies in the range of 0 to 0.9 A while there is no effect on the speed of the rotor.

When the solar irradiance reduces to 0  $\text{w/m}^2$ , the PV voltage and dc output voltage are 0.005 and 360 V, respectively, while the current falls to 0 A, which is quite apparent. In this condition, the battery's voltage is observed at 323.4 V while the battery's current falls to 2.5 A and flows in the reverse direction. The bidirectional's converter current varies in the range of 0 to 3 A, also in the reverse direction, verifying the design. There is no effect on the speed of the rotor.

The performance of the solar-based ACS is found to be satisfactory with constant speed despite the variation of solar irradiance, which verifies the design and sustainability. Hence, the designed solar-based ACS is a recommendable solution to replace the conventional supply-based ACS.

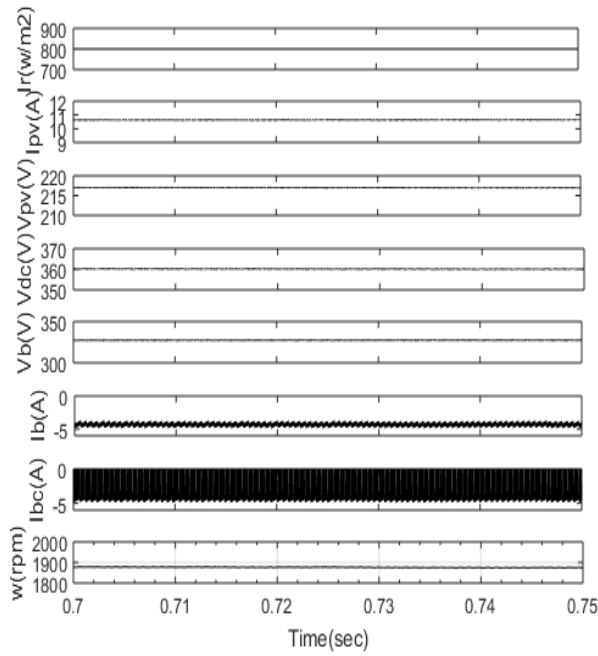


Fig. 6. PV current, PV voltage, PV power, dc output voltage, battery charge controller voltage, current, and bidirectional converter current at solar irradiance( $G=800 \text{ w/m}^2$ ).

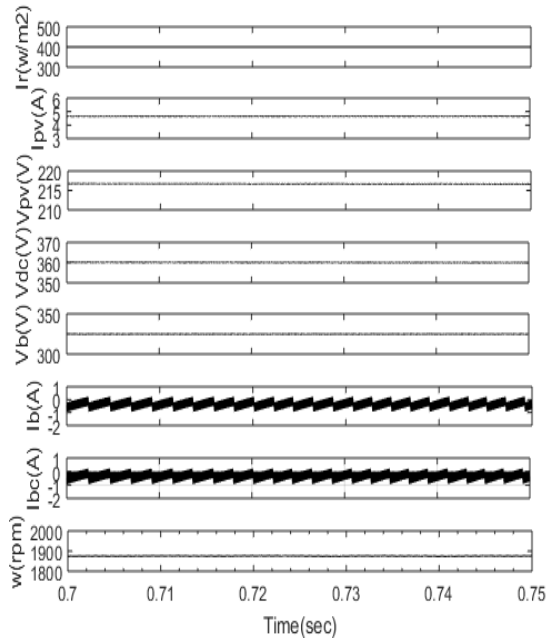


Fig. 7. PV current, PV voltage, PV power, dc output voltage, battery charge controller voltage, current, and bidirectional converter current at solar irradiance( $G=400 \text{ w/m}^2$ ).

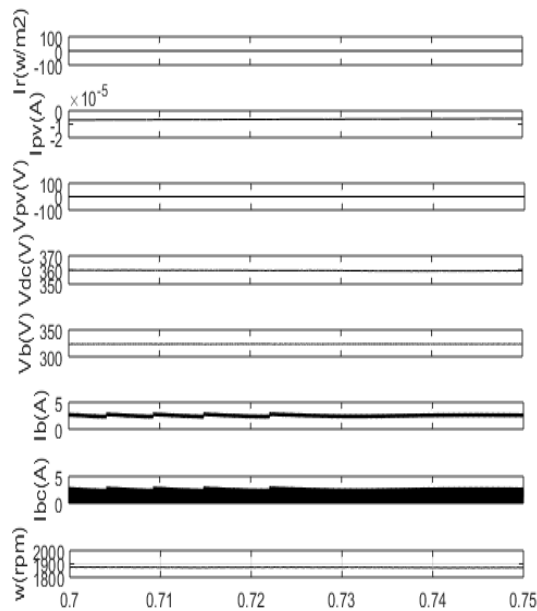


Fig. 8. PV current, PV voltage, PV power, dc output voltage, battery charge controller voltage, current, bidirectional converter current, and speed at solar irradiance( $G=0 \text{ w/m}^2$ ).

Table 4 shows the different parameters for the variation of solar irradiation from  $1000 \text{ w/m}^2$  to  $0 \text{ w/m}^2$ .

Table 4. Various parameters for the variation of solar irradiance.

Solar Irradiance (w/m2)	$V_{PV}(V)$	$I_{PV} (A)$	$V_{dc}(V)$	$V_b(V)$	$I_b(A)$	$I_{bc}(A)$	$\omega(\text{rpm})$
1000	217	13.58	360	329	6.2	6.6	1874
800	217	10.64	360	327	4.3	4.8	1874
600	216.8	7.66	360	326	3.7	2.85	1875
400	216.7	4.65	360	325	0.5	0.9	1875
0	0.005	0	360	323.4	2.5 (reverse)	3 (reverse)	1878

### 5. Conclusion

The solar-based ACS has been designed, and its performance has been assessed through design and simulation under varying solar irradiance to demonstrate its reliable operation. Solar PV has been used as an energy source to operate the ACS despite conventional AC supply. The boost converter tracks the MPP, while the battery along with the converter maintains the voltage when solar irradiation is not present, which has been presented through the simulated performance of the ACS. The speed & torque of solar-based ACS is constant, which is the prime requirement in the ACs. Hence, it is recommended as a solution to conventional supply, which removes the harmonic pollution problem of a conventional system and so reduces the effect of carbon emission.

**References**

1. Ministry of New and Renewable Energy, Government of India (2015-2016)
2. G. Yang, J. K. Zimmermann, K. H. B. Frederiksen, T. Helth, H. H. Ipsen, T. V. Hansen, and S. B. Kjaer - 7<sup>th</sup> *Int. Conf. on Renewable Power Generation*, **18** (2019).  
<https://doi.org/10.1049/joe.2018.9244>
3. R. Foster, M. Ghassemi, and A. Cota, *Solar Energy Renewable Energy and the Environment* (CRC Press, New York, 2010). <https://doi.org/10.1201/9781420075670>
4. R. Z. Wang and T. S. Ge, *Advances in Solar Heating and Cooling* (Woodhead Publishing, 2016).
5. M. J. H. Munshi and M. A. Alim, *J. Sci. Res.* **9**, 1 (2017).  
<https://doi.org/10.3329/jsr.v1i1.27702>
6. S. H. Islam, P. Begum, and D. Sarma, *J. Sci. Res.* **13**, 1 (2021).  
<https://doi.org/10.3329/jsr.v13i1.48174>
7. B.A. Allah and L. Djamel, *Int. J. Electr. Computer Eng. (IJECE)* **6**, 1 (2016). <https://doi.org/10.11591/ijece.v6i1.8632> .
8. S. Murshid and B. Singh, *IEEE Trans. Industry Appl.* **56**, 4, (2020).  
<https://doi.org/10.1109/TIA.2020.2988429>
9. H. Liu, H. Hu, H. Wu, Y. Xing, and I. Batarseh, *IEEE J. Emerging Selected Topics Power Electronics* **4**, 2 (2016). <https://doi.org/10.1109/JESTPE.2016.2532930>
10. H. Gupta, P. Gajera, and V. Gupta – *Int. Conf. on Power Electronics & IoT Applications in Renewable Energy and Its Control (PARC)* (GLA University, Mathura, 2020), pp.70-74.  
<https://doi.org/10.1109/PARC49193.2020.246973>
11. S. Navinchandran and M. Sujith – 4<sup>th</sup> *Int. Conf. on Inventive Systems and Control (ICISC)* (2020) pp. 363-368. <https://doi.org/10.1109/ICISC47916.2020.9171133>
12. J. Thankachan, and S. P. Singh, *IET Electr. Power Appl.* **14**, 4 (2019).
13. D. Sha, T. Sun, and J. Zhang, *IEEE Trans. Power Electron.* **35**, 4 (2020).  
<https://doi.org/10.1109/TPEL.2019.2938779>
14. V. K. Singh, Y. Sahu, P. K. Mishra, P. Tiwari, and R. Maurya – *Int. Conf. on Electrical and Electronics Engineering (ICE3)* (2020) pp. 82-88.  
<https://doi.org/10.1109/ICE348803.2020.9122843>
15. R. Teodorescu, M. Liserre, and P. Rodriguez, *Grid Converters for Photovoltaic and Wind Power Systems*, 1<sup>st</sup> Edition (John Wiley, United Kingdom, 2011).  
<https://doi.org/10.1002/9780470667057>
16. R. M. Sallinen and T. Messo, *J. Eng.* **18**, 5197 (2019). <https://doi.org/10.1049/joe.2018.9332>
17. M. N. Bhukya, V. R. Kota, and S. R. Depuru, *IEEE Access* **7**, 43831 (2019).  
<https://doi.org/10.1109/ACCESS.2019.2902979>
18. H. Wang, W. Wu, S. Zhang, Y. He, H. S. H. Chung, and F. Blaabjerg, *Transact. Power Electron. Applicat.* **4**, 2 (2019). <https://doi.org/10.24295/CPSTPEA.2019.00011>
19. S. Madichetty, D. Pullaguram, and S. Mishra, *J. Power Energy Syst.* **5**, 1 (2019).  
<https://doi.org/10.17775/CSEEJPES.2018.00410>
20. N. Pachaivannan, R. Subburam, U. Ramkumar, and P. Kasinathan, *IET Renew. Power Gener.* **13**, 12 (2019). <https://doi.org/10.1049/iet-rpg.2018.5053>
21. C. J. O. Junior, L. P. Pires, L. C. Freitas, E. A. A. Coelho, G. B. Lima, and L. C. G. Freitas, *IET Power Electron.* **11**, 1 (2017). <https://doi.org/10.1049/iet-pel.2017.0342>
22. A. H. Elmetwaly, A. A. Eldesouky, and A. A. Sallam, *IEEE Access* **8**, 57923 (2020).  
<https://doi.org/10.1109/ACCESS.2020.2981444>
23. S. J. Alam and S. Raj Arya, *Chinese J. Elec. Eng.* **6**, 2 (2020).  
<https://doi.org/10.23919/CJEE.2020.000011>
24. H. Luo, J. Xu, Y. Luo, and J. Sha, *IEEE Trans. Ind. Electron.* **66**, 4 (2019).  
<https://doi.org/10.1109/TIE.2018.2842776>

25. K. Akter, G. Sarowar, M. A. Hoque, and S. F. B. Ahmed - *4<sup>th</sup> Int. Conf. on Electrical Engineering and Information & Communication Technology (ICEEICT)*, (2018) pp. 240-245. <https://doi.org/10.1109/CEEICT.2018.8628168>
26. B. R. Ananthapadmanabha, R. Maurya, and S. R. Arya, *IEEE Trans. Power Electron.* **33**, 11 (2018). <https://doi.org/10.1109/TPEL.2018.2797005>
27. H. Ma, Y. Li, J. S. Lai, C. Zheng, and J. Xu, *IEEE J. Emerging Selected Topics Power Electron.* **6**, 3 (2018). <https://doi.org/10.1109/JESTPE.2017.2768545>
28. X. Lin and F. Wang, *IEEE Trans. Ind. Electron.* **65**, 10 (2018). <https://doi.org/10.1109/TIE.2018.2801782>
29. B. Das, S. Banerjee, S. Kumar, P. R. Kasari, and A. Chakrabarti - *IEEE Int. Conf. on Power Electronics, Drives and Energy Systems (PEDES)* (2019) pp. 1-5. <https://doi.org/10.1109/PEDES.2018.8707873>